Catalysis Today 202 (2013) 98–104

Contents lists available at SciVerse ScienceDirect

Catalysis Today

journal homepage: www.elsevier.com/locate/cattod

Theoretical modeling of electrode/electrolyte interface from first-principles periodic continuum solvation method

Ya-Hui Fang[a,b], Guang-Feng Wei[b], Zhi-Pan Liu[b,*]

[a] School of Chemical and Environmental Engineering, Shanghai Institute of Technology, Shanghai 201418, China
[b] Shanghai Key Laboratory of Molecular Catalysis and Innovative Materials, Department of Chemistry, Key Laboratory of Computational Physical Science (Ministry of Education), Fudan University, Shanghai 200433, China

ARTICLE INFO

Article history:
Received 22 November 2011
Received in revised form 13 February 2012
Accepted 23 April 2012
Available online 4 June 2012

Keywords:
Electrochemistry
First principles periodic continuum solvation method
Potential of zero charge
Differential capacitance
CO electrooxidation

ABSTRACT

It has been a long challenge to understand the equilibrium and the dynamic phenomena (e.g. chemical reactions) at the electrode/electrolyte interface in a unified theoretical framework. Here periodic first-principles calculations integrated with modified-Poisson–Boltzmann electrostatics are utilized to provide the atomic level insight into the nature of electrochemical double layer and the catalytic reaction at the interface. The double layer properties of a series of metal electrodes and CO-covered Pt electrode, such as the potential of zero charge and the differential capacitance, are calculated from theory and a good agreement between theoretical values and experimental data is achieved. The theoretical method is also applied to understand the mechanism of CO electrooxidation on Pt. By comparing CO + O and CO + OH reaction channels, we show that CO + OH is the major mechanism for CO electrooxidation. It is observed that the barriers of these surface association reactions are weakly dependent on the potential. The theoretical results presented here demonstrate that first-principles periodic continuum solvation method is a practical and general-purpose theoretical tool for studying electrochemical phenomena occurring at the electrode/electrolyte interface.

1. Introduction

The electronic and geometrical structure of the electrode/electrolyte interface lies at the heart of the electrochemical processes. The current knowledge on the electrochemical double layer originates mainly from the measurement of the macroscopic, equilibrium properties of the interface, such as surface tension, work function and interfacial capacitance [1–6], and also the simplified theoretical model based on classical Poisson–Boltzmann electrostatics from Gouy–Chapmann and Stern [7–9] (GCS model). Due to the electrochemical adsorption, the redox reactions involving water and electrolyte, and the surface structural reconstruction (defect creation), especially on active transition metals, it is generally difficult to measure accurately the double layer properties. For instance, for the typical catalyst in fuel cell, Pt electrode, the potential of zero charge (pzc) and differential capacitance (C_d) have been measured with different experimental methods and the reported values span a certain range (pzc: 0.2–0.4 V and C_d: 14–20 μF/cm^2 [10–12]). In line with this, the understanding for the electrocatalytic reactions that occur at the electrode/electrolyte interface is much poorer compared to those for the solid–gas reactions, not least because of the complexity of the electrode/electrolyte interface. New experimental and theoretical techniques are urgently required to decouple the many-body problem associated with the electrode/electrolyte interface, where the electrochemical potential, the adsorbate, the surface structure and the solution are the key factors.

Recent years have seen a great progress in understanding electrochemical phenomena using theoretical methods, such as Canonical Monte Carlo [13], Wertheim–Lovett–Mou–Buff integral equation [14,15], modified Poisson–Boltzmann (MPB) [16–18] and molecular dynamics [19–22]. As one of the major progress, the solid-liquid interface can now be studied with the state-of-the-art quantum mechanics approaches, such as the large-scale density functional theory (DFT) calculations [23–25]. Neurock and coworkers proposed a double-reference method to describe the metal/water interface, in which the water layers outside the metal surface are explicitly included with the ice-like structure and the counter charge of electrolyte is described by the homogenously distributed background charge [24,26]. Using Cu(1 1 1) in contact with water as the model, they calculated pzc (0.6 ± 0.1 V vs. SHE, cf. exp. −0.01 V [27]) from the double-reference method [28], but there are still obvious difference between theory and experimental values. By fitting the curvature of the parabola of free energy versus potential, Norskov group [25] calculated C_d of Pt(1 1 1) with a few layers (1–3) explicit water included and the calculated value 23 μF/cm^2

* Corresponding author.
E-mail address: zpliu@fudan.edu.cn (Z.-P. Liu).

0920-5861/$ – see front matter © 2012 Elsevier B.V. All rights reserved.
http://dx.doi.org/10.1016/j.cattod.2012.04.055

is somewhat larger than the reported experimental value [10–12]. They also investigated hydrogen oxidation and evolution reaction with a water bi-layer model by adding protons into the first water layer [25]. Recently, a periodic continuum-solvation method based on the modified-Poisson–Boltzmann theory [16] has been implemented in DFT framework (DFT/CM-MPB) for modeling the electrode/solution interface [29,30]. Jinnouchi and Anderson analyzed the pzc of Pt(1 1 1) with different water coverage and water orientation with the values from −0.35 to 0.74 V [29,31]. They found that the exact water orientation can affect greatly the pzc. This is consistent with the conclusion obtained from other research groups with water bilayer on metals: it was found that the work function difference between the H-down and H-up water bilayer structure on Pt(1 1 1) can be as large as 2.6 eV [25]. By focusing on the dynamic aspects of the reaction, our group recently investigated water splitting on RuO_2 and TiO_2 under electrochemical and photocatalytic conditions [30,32].

To date, it remains unclear whether it is possible to treat the static/equilibrium (such as pzc, C_d) and the dynamic properties (chemical reactions) of the electrode/electrolyte interface in a unified theoretical framework. One may be able to predict the static properties of the interface via heavy demanding computational techniques such as first principles molecular dynamics, but these methods are not practical in general for studying the rare dynamic event (reactions) under electrochemical condition. In this work, we demonstrate that the theoretical approach based on periodic DFT/CM-MPB calculations can be utilized to model electrochemical interface and the effects due to the solvation and the electrochemical potential can be included straightforwardly. We calculate the equilibrium properties of the double layer of a series of metal electrodes and CO-covered Pt electrode. We also apply the method for understanding a typical reaction on Pt electrode, i.e. CO oxidation. The results from theory are compared thoroughly with those from the experimental measurement.

2. DFT calculation detail

All DFT calculations were performed using SIESTA package with numerical atomic orbital basis sets and Troullier–Martins norm-conserving pesudopotentials [33–35]. The exchange-correlation functional utilized was at the generalized gradient approximation level, known as GGA-PBE [36]. The optimized double-ζ plus polarization basis (DZP) set was employed routinely for total energy calculations and the diffuse basis (e.g. 7s for Au) was also added in calculating work function of metal surfaces [37]. The orbital-confining cutoff was determined from an energy shift of 0.010 eV. The energy cutoff for the real space grid used to represent the density was set as 250 Ry. The Quasi-Newton Broyden method was employed for geometry relaxation until the maximal forces on each relaxed atom were less than 0.1 eV/Å. Transition states (TSs) of the catalytic reaction were searched using our recently developed Constrained-Broyden-Minimization [38] and the Constrained-Broyden-Dimer methods [39]. In all calculations, the rectangular $p(4 \times 2\sqrt{3})$ symmetric six-layer slab was utilized routinely for modeling the (1 1 1) surfaces and the middle two layers were fixed at the bulk-truncated position. The adsorbates were added symmetrically on both sides of the slab. To compute Pt(1 1 1) at various CO coverage conditions and the CO oxidation reaction, both $p(2 \times 2\sqrt{3})$ and $p(4 \times 2\sqrt{3})$ unit cells were utilized.

3. Periodic continuum-solvation method based on modified Poisson–Boltzmann equation

In our previous work, we have developed a Gaussian-plane-charge method for the calculation of charged surfaces [40] (the counter-charge is distributed in a Gaussian-plane several angstroms away from the surface), which considers the surface polarization explicitly due to the surface charging. However, because of the lack of solvation and the unrealistic ionic charge distribution, the Gaussian-plane-charge method is not ideal for an accurate description of electrocatalytic reaction. Recently, we replace the Gaussian-plane charge distribution by a point-charge distribution in the continuum dielectric medium throughout the entire vacuum region (at the grid points in DFT calculations), which mimics the real ionic distribution of electrolyte [41]. This approach is introduced below.

3.1. Continuum solvation

The continuum dielectric medium is introduced via a parameterized smooth dielectric function $\varepsilon(r)$ (Eq. (1)) as proposed by Fattebert and Gygi [42],

$$\varepsilon(\rho(r)) = 1 + \frac{\varepsilon_\infty - 1}{2}\left[1 + \frac{1-(\rho(r)/\rho_0)^{2\beta}}{1+(\rho(r)/\rho_0)^{2\beta}}\right] \quad (1)$$

which approaches to ε_∞ (e.g. 78.36 for water at room temperature) asymptotically in the regions where electron density is low, and 1 in the regions where it is high. In the equation, ρ_0 and β are the only two parameters: ρ_0 is the threshold of electron density $\rho(r)$ to adjust the size of the cavity, whereas β determines the smoothness of the transition from 1 to ε_∞. According to Fattebert and Gygi, these two parameters can be chosen by fitting the experimental solvation energy value for the systems of interest (e.g. water) and the values utilized in this work is 5.5 e/bohr^3 for ρ_0 and 1.3 for β. For $\rho(r)$, we utilize the pseudoatomic charge distribution according to the pre-defined atomic configuration of the element and it is then fixed during the self-consistent loop. A fixed $\varepsilon(r)$ during the self-consistent field calculation is found to be essential to speed up the convergence, especially for metallic system. The atomic configuration of the element acts as a convenient way to tune the solvation radius of the element, similar to that utilized in traditional continuum solvation method [43]. The continuum solvation model enables the band structure alignment between different surfaces with the same solution level (i.e. the potential zero defined in the middle of the vacuum of slab where the dielectric function approaches to 78.36), and more importantly, it corrects the DFT energy with the long-range electrostatic interaction due to solvation.

For example, the typical distribution of $\varepsilon(r)$ for a metal surface (Pt(1 1 1)) at different atomic configurations are shown in Fig. 1a, where the dielectric function increases from 1 (metal bulk) to 78.36 (water solution) within a thickness of ~3 Å from the surface plane. By changing the atomic configuration, the distribution of dielectric function $\varepsilon(r)$ is also modified: as seen in Fig. 1a, with the gradual depopulation of electrons in 5d, the solution (ε = 78.36) will be pushed away from the surface. Consistently, we found that the potential of zero charge (pzc) will increase gradually. The calculated pzc are 0.31, 0.50, 0.60, 0.71 with the Pt atomic configuration $5d^{10}6s^0$, $5s^96s^1$, $5s^86s^2$, $5d^76s^26p^1$, respectively (see Section 4.1 for more detail), indicating that the pzc is very sensitive to the exact solvation radius of the element.

3.2. MPB implementation in slab calculations

We utilize the MPB equation as shown in Eq. (2) [16,18] to determine the total electrostatic potential, where k *is* the Boltzmann constant, T is the absolute temperature, and $\nu = 2a^3c_b$ (a is the effective ion size and c_b is the bulk concentration of the electrolyte). The technique detail for the implementation of the numerical PB solver in periodic slab calculations was described in our previous work

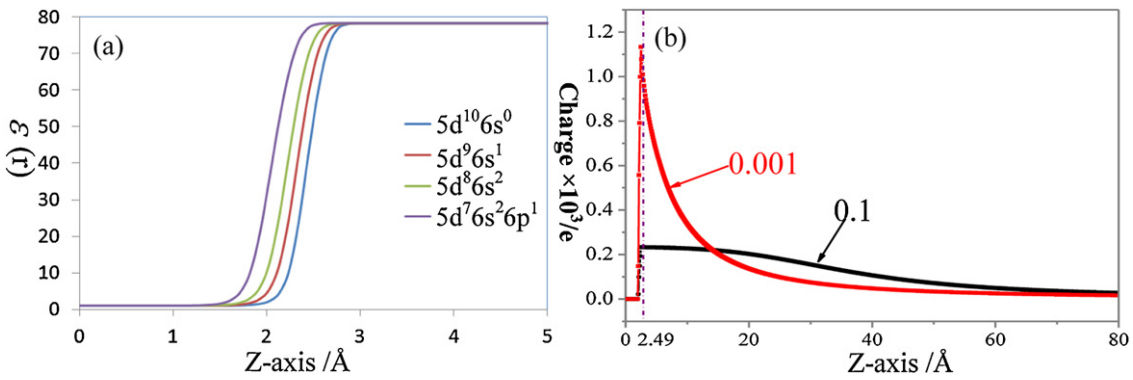

Fig. 1. (a) The dielectric function $\varepsilon(r)$ profile as a function of the z-axis of the supercell, which can be tuned by modifying the atomic configuration of the element; (b) an example showing the ionic charge distribution ($q = 0.2|e|$) as determined from MPB equation (red line: $\nu = 0.001$, black line: $\nu = 0.1$, see Eq. (2)). With $\nu = 0.1$ (the larger ionic size), one can see the fast saturation of ionic charge concentration at the distance close to the surface. Both (a) and (b) are obtained from Pt(1 1 1) slab calculation, where the surface plane locates at the zero in z-axis. (For interpretation of the references to color in this figure legend, the reader is referred to the web version of the article.)

[41,44]. In short, we utilize a sixth-order finite-difference scheme that is appropriate to discretize partial differential equations with periodic boundary condition [45], which is solved numerically in the self-consistent loop. This scheme utilizes the finite difference stencil to get the symmetric sparse linear system. In terms of the symmetry, the linear system is solved iteratively by a parallel version of MINRES with the preconditioner. To realize a fully parallelism, we chose the incomplete LU preconditioners based on the second-order FD scheme in a localized preconditioner implementation. Generally, a large vacuum region along Z axis is needed to separate two adjacent slabs.

$$\nabla \cdot (\varepsilon(r))\nabla(\psi) = -4\pi\rho + 8\pi z e c_b \frac{\sinh(ze\psi/kT)}{1 - \nu + \nu\ \cosh(ze\psi/kT)} \tag{2}$$

$$q = -\int dr \cdot \rho_{cq}(r)\Big|_{\varepsilon(r)>\alpha} \tag{3}$$

$$\rho_{cq}\Big|_{\varepsilon(r)<\alpha} = 0 \tag{4}$$

$$U^{q}_{cal} = (\Phi_{ref} - \Phi_F) - 4.6 \tag{5}$$

The Boltzmann distribution of the ionic charge (i.e. countercharge) is determined by the second term in the right-hand side of Eq. (2), which can be solved self-consistently during electronic structure loops with the constraint of the total charge conservation as written in Eqs. (3) and (4) (ρ_{cq} is the countercharge density, q is the net charge of the surface, the parameter α defines the region that is not accessible to the ionic charge). A critical parameter in MPB is ν, which describes the size effect of ionic charge in solution. By changing ν, the charge distribution will be altered and a representative result for the distribution of the ionic countercharge is shown in Fig. 1b. In this work, ν is set as 1×10^{-3} by assuming $c_b = 0.1$ mol/L, $a = 2$–4 Å and $z = 1$ for typical 1:1 electrolytes [18]. In the calculations with net surface charge, we set $\alpha = 19.59$ (=78.36/4) in Eqs. (3) and (4), which effectively excludes the ionic charge of electrolyte from penetrating into the metal surface and allows the charge conservation in the whole slab. Using the MPB solver, we can calculate the electrochemical potential U^{q}_{cal} of a system with a net charge q referring to SHE (~4.6 V according to experiment [46]) using Eq. (5), where the computed work function in solution ($\Phi_{ref} - \Phi_F$) defined as the potential difference between the Fermi Level Φ_F and the potential level in solution Φ_{ref}.

4. Results and discussion

4.1. pzc of metal surfaces

The pzc is a fundamental property of the solid/electrolyte interface, defined as the value of the electrochemical potential of an electrode (against a defined reference electrode) when the surface charge is zero. Trasatti and Lust [27] pointed out that pzc is influenced by both the orientation of dipole moment of solvent molecules and the changes in the metal surface dipole due to the contact with solution. The pzc of Pt group metals have been studied intensively in experiment, which can serve as a good dataset for comparison with theoretical calculations [47,48].

Theoretically, it is possible to calculate the pzc by using Eq. (5) with $q = 0$. In this work, the workfunction of six typical late transition metal surfaces in vacuum and solution, namely Pt(1 1 1), Pd(1 1 1), Ir(1 1 1), Rh(1 1 1), Au(1 1 1) and Ag(1 1 1), have been investigated. The calculated workfunction in vacuum and pzc are listed in Table 1 and the experimental values are also compared. The dielectric function distribution of the DFT/CM-MPB model is calculated based on the pseudoatomic charge density according to the pre-defined atomic configuration of the element, which is also listed in Table 1. We found that the pzc for metal surfaces determined from the DFT/CM-MPB method are in general consistent with experimental data (no specific adsorption of anions). The solvation energy gain calculated for the metal surfaces are small, being −0.01 to −0.1 eV per surface atom. For 5d metals Pt(1 1 1) and Ir(1 1 1), the solvation energy is the largest, being ~−0.07 eV per atom, and the decrease of the workfunction from the vacuum to solution is therefore the largest, about 0.6 V. In contrast, the coinage metals (Au, Ag) have weakest interaction with water and thus have the lowest solvation energy per atom. Consistently, the workfunction of them in solution is quite close to that in vacuum (the differences are within 0.3 V from theory).

It should be mentioned that the DFT-PBE workfunction in vacuum of metals are in general lower than the experimental values up to several tenth eV [37,49,50]. The good agreement between theoretical pzc and experimental values should therefore be treated with caution. Considering that there are several parameters involved in the DFT/CM-MPB calculations (i.e. two parameters in dielectric function distribution and the atomic configuration of element), we expect that the error cancellation occurs in computing pzc, and therefore the trend across metals might be more meaningful. It is important that pzc calculations as we did here can be utilized to assess the validity of the parameters in MPB model, which is the key step for applying the MPB method in other applications, for example, the catalytic reactions at the interface.

Table 1
The workfunction (Φ) and pzc of Pt-group metal surfaces.

Metal	Φ/eV[a]	pzc/V[a]	E_{solv}/eV[b]	Atomic configuration
Au(1 1 1)	5.19 (5.47)	0.34 (0.47–0.58)	−0.029	$5d^9 6s^2$
Pt(1 1 1)	5.52 (5.93)	0.31 (0.2–0.4)	−0.071	$5d^{10} 6s^0$
Ir(1 1 1)	5.25 (5.76)	0.00 (0.01–0.13)	−0.067	$5d^9 6s^0$
Ag(1 1 1)	4.51 (4.74)	−0.39 (−0.45)	−0.015	$4d^9 5s^2$
Pd(1 1 1)	5.395 (5.6)	0.247 (0.20)	−0.049	$4d^{10} 5s^0$
Rh(1 1 1)	5.03 (5.3)	0.01 (0.05–0.12)	−0.038	$4d^8 5s^1$

[a] The data in parenthesis are the experimental values (taken from [50,27,51] and references therein).
[b] E_{solv} is the calculated solvation energy per surface atom.

To provide deeper insight into the solvation effect of metal surface, we have examined the electronic structure of Pt(1 1 1) system with and without the solvation by analyzing the total electrostatic potential. The solvation effect can be visualized by plotting the change of total electrostatic potential on moving from the vacuum to the solution. Fig. 2 shows evidently that Pt surface is strongly polarized by solvation, which places a net positive electrostatic field on the surface and effectively decreases the workfunction of the surface. In response to the positive electrostatic field, the extra electron will accumulate onto the surface and help to stabilize the surface (reduce surface energy).

4.2. Differential capacitance

The differential capacitance C_d (=$\partial\sigma/\partial U$) is also an important parameter introduced for characterizing the electrical double layer, which reflects the ability of electrode surface to store charges (σ) in response to the perturbation of potential. Within the DFT/CM-MPB framework, we can charge metal surface explicitly with different surface charges (e.g. from −5 to +5 μC/cm^2) and the potential of the surface (vs. SHE) was then obtained by measuring the work function in solution as described by Eq. (5). Because the ionic charge density of electrolyte converges rather slowly to the bulk concentration with the increase of the distance to the electrode surface (defined as z-length, i.e. the vacuum thickness in the slab modeling), we have compared the calculated C_d with different z-length up to 200 Å. In Fig. 3a the potential is plotted against the surface charge density (σ) for Pt(1 1 1) surface at different z-lengths and the differential capacitance C_d can then be obtained by fitting the slop of $\sigma \sim U$, as drawn in Fig. 3b.

Fig. 3 shows that the excess charge and the electrochemical potential are intimately correlated and the increase of the surface excess charge can elevate the electrochemical potential of the system. Importantly, for small z-lengths, e.g. below 50 Å, the $\sigma \sim U$ curve is essentially a straight line with a constant C_d being about 20 μF/cm^2. For large z-lengths, e.g. above 150 Å, the $\sigma \sim U$ curve starts to exhibit a flat region nearby the pzc, which correctly describes the slow variation of ionic concentration at the (low) potential regions nearby pzc. Consistently, C_d will show a minimum at the pzc and it rises rapidly to ~20 μF/cm^2 as the potential moves away from pzc. Our calculated value for C_d agrees with ~20 μF/cm^2 for double layer from experiment for Pt(1 1 1) surface [11,12,47,48]. The dependence of $\sigma \sim U$ curve on the vacuum length can be understood as follows. In our implementation, we confine the ionic charge (counter charge) in the vacuum region by the charge conservation constraint (Eq. (3)). At the low potentials (near pzc), the ionic charge is rather diffusing and decays very slowly to the bulk concentration in reality, which requires a large solution length for distributing the ionic charge. As a result, the small vacuum length cannot produce correctly the distribution of the ionic charge distribution. On the other hand, the vacuum thickness does not affect significantly the limiting value of C_d at the high potentials and pzc. In the former case, the distribution of ionic counter charge decays rapidly, whilst the ionic counter charge is zero at pzc.

The C_d of electrode can be derived from GCS double layer model (C_{GCS}). Based on the GC model from electrostatics and statistic

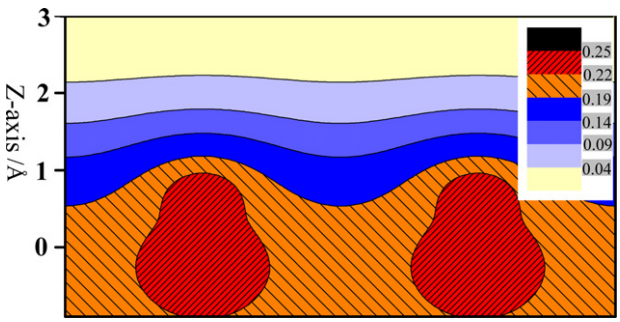

Fig. 2. The contour plot for the change of the total electrostatic potential (ESP) induced by solvation, constructed by subtracting the ESP of a nonsolvated surface from that of a solvated system using CM-MPB. The position of the surface plane is set as zero in z-axis (normal to surface plane).

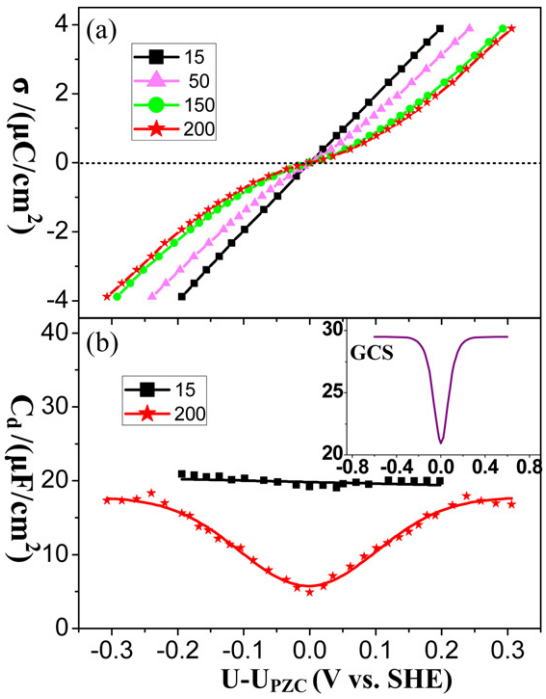

Fig. 3. (a) The charge density versus potential ($\sigma \sim U$) curves of Pt(1 1 1) surface from CM-MPB model with different z-length (vacuum thickness in slab calculation), i.e. 15, 50, 150 and 200 Å and (b) the C_d versus potential curve on Pt(1 1 1) from CM-MPB model. The insert in (b) shows the $C_d \sim$ potential curve from GCS model. The drop of C_d is caused by the slow variation of ionic concentration at the potential around pzc: the ionic charge decays slowly to the bulk concentration at the potentials around pzc but very rapidly at the high potentials. Therefore, only a large vacuum in slab calculations can capture this fine detail of C_d drop, as shown in (b). On the other hand, the vacuum thickness does not affect significantly the limiting value of C_d and pzc.

mechanics, Stern suggested an important modification, where the Stern model considers the finite size effect of ions which cannot approach to the surface any closer than the ionic radius. The overall capacitance can be written as the reciprocals of component capacitances, C_H and C_D, where the C_H corresponds to the capacitance of the charges held at the outer Helmholtz plane (OHP), and C_D is the capacitance of the truly diffuse charge, as expressed in Eqs. (6) and (7). In the equations, x_2 is the thickness of OHP (typically 3 Å), z is the charge of ion, n^0 is number concentration of ion in a z:z electrolyte and φ_0 is the potential drop across the diffuse layer. For dilute aqueous solution at 25 °C, Eq. (7) can be simplified as Eq. (8), where the unit of C_d is μF/cm^2 and that for c_b, the bulk electrolyte concentration, is mol/L (see Ref. [1] for detail). Using Eq. (9), we can derive the C_d value of the GCS model. By using x_2 = 3 Å, ε = 10 (suggested from experiment [52,53]), c_b = 0.1 mol/L and z = 1 for typical 1:1 electrolytes, we have plotted the $C_{GCS} \sim U$ curve in the insert of Fig. 3b. Clearly, the drop of capacitance at the pzc region is correctly described by the GCS model.

$$C_H = \frac{\varepsilon\varepsilon_0}{x_2} \tag{6}$$

$$C_D = \left(\frac{2z^2e^2\varepsilon\varepsilon_0 n^0}{kT}\right)^{1/2} \cosh\left(\frac{ze\varphi_0}{2kT}\right) \tag{7}$$

$$C_D = 228zc_b^{1/2} \cosh(19.5z\varphi_0) \tag{8}$$

$$\frac{1}{C_{GCS}} = \frac{1}{C_H} + \frac{1}{C_D} = \frac{x_2}{\varepsilon\varepsilon_0} + \frac{1}{228zc_b \cosh(19.5z\varphi_0)} \tag{9}$$

Seen from Fig. 3, obviously, the current DFT/CM-MPB model yields more reasonable C_d values (~20 μF/cm^2), while the GCS model's prediction is large (~30 μF/cm^2) when comparing with experimental values. The rapid increase of C_d with the increase of potential away from pzc predicted by the GCS model is quite similar to that calculated from DFT/CM-MPB model, and is consistent with typical experimental C_d curve [e.g. Hg [54]]. Obviously, the DFT/CM-MPB model treatment of the metal electrode surface can describe the electrical double layer with good accuracy provided with the suitable MPB solvation parameters. Especially the diffuse surface charges and their explicit polarization under the influence of solvation can now be described within the same framework of DFT slab calculations. This is important considering that one can go further to study more complex interface properties using DFT/CM-MPB model without recourse to further experimental information.

4.3. CO adsorbates and catalytic reactions

It is of significance to extend the current DFT/CM-MPB model for treating the realistic catalytic environment under which chemical reactions occur. In reaction conditions, the adsorption of reaction intermediates will modify the interface properties (such as pzc, C_d) and the theoretical model should be able to describe correctly the change of the double layer properties induced by adsorbates. The major challenge in theory is therefore to treat the solvation of small molecule adsorbates together with the extended electrode with an equal footing. Since CO on transition metal surface is a model system in electrochemistry and a large volume of experimental data are available for comparison [55–57], we investigated the interface properties of CO adsorbed Pt(1 1 1) under the framework of DFT/CM-MPB. The theoretical pzc and C_d are calculated with different CO coverages and adsorption geometry on Pt(1 1 1).

The adsorption of CO on Pt single crystal surfaces has been investigated by different electrochemical techniques, such as IR spectroscopy, in situ STM, coupled UHV-electrochemistry techniques and in situ X-ray diffraction [58–60]. It is now well established that the saturation coverage of CO (θ_{CO}) on Pt(1 1 1)

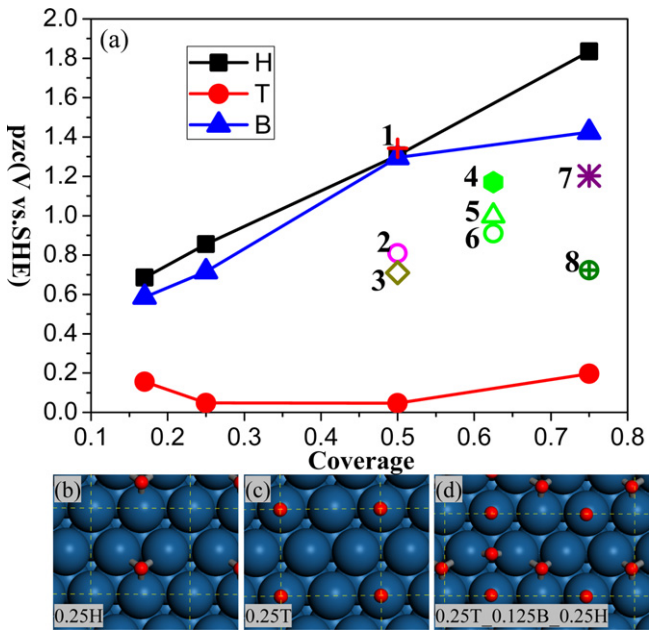

Fig. 4. (a) The calculated pzc versus CO coverage curves for CO covered Pt(1 1 1) surface. T, B, H stand for top, bridge and hollow sites for CO adsorption, respectively. The structures with mixed CO adsorption sites are indicated by numbers **1**–**8** and their meaning is as follows. **1**: 0.25B_0.25H (i.e. 0.25 ML bridge CO plus 0.25 ML hollow CO); **2**: 0.25T_0.25H; **3**: 0.25T_0.25B; **4**: 0.125T_0.25B_0.25H; **5**: 0.25T_0.125B_0.25H; **6**: 0.25T_0.25B_0.125H; **7**: 0.25T_0.25 B_0.25H; **8**: 0.5T_0.25H. (b) 0.25 ML CO at the hollow site; (c) 0.25 ML CO at the top site; (d) 0.625 ML CO at hollow (0.25 ML), bridge (0.125 ML) and top (0.25 ML) sites.

electrode is 0.75 ML at low electrochemical potential (<0.25 V), corresponding to a $c(2 \times 2)$-3CO structure, comprising of CO at both the atop site (denoted as T) and threefold fcc hollow sites (denoted as H) (see Fig. 4). At the potential above 0.25 V, this adsorption structure converts to a ($\sqrt{19} \times \sqrt{19}$)-R23.4 structure ($\theta_{CO}$ = 0.68), where CO adsorption at the bridge site (denoted as B) is also observed in addition to the top and hollow sites.

From a theoretical point of view, it is possible to calculate the pzc and C_d values at different CO coverage conditions and map out the relationship between CO coverage/adsorption structures with the double layer properties. By calculating the pzc value of various CO/Pt(1 1 1) systems as shown in Fig. 4, we found that the three quantities, namely coverage, adsorption site and pzc are closely related, in particular, CO adsorption site can have a great impact on the pzc. Taking 0.17 ML CO as the example, CO at the threefold fcc site exhibits the highest pzc, 0.69 V and that follows the CO at the bridge sites, 0.59 V. The top site adsorption geometry exhibits the lowest pzc of only 0.16 V. This is a reflection of the fact that the workfunction of a surface is sensitive to the adsorbate and their adsorption site. For CO adsorption, owing to its bi-bonding mode, i.e. 5σ donation and 2π backdonation, the surface dipole is rather sensitive to CO adsorption geometry. The hollow site adsorption geometry will induce a higher degree of the 2π backdonation compared to the top site adsorption structure and thus lead to a larger increase of workfunction. Further increasing the CO coverage, we found that interestingly, the pzc values corresponding to CO at the threefold hollow sites and bridge sites will increase rapidly with the increase of the coverage, while those corresponding to the top site remain rather constant below 0.2 V. It is therefore expected that both the CO adsorption site and the coverage are critical to the pzc of CO/metal system.

To compare with the experimental data with high CO coverages, we then studied a set of CO adsorption structures at high coverages, namely three structures at 0.5 ML, three at 0.625 ML and two at 0.75 ML, and all comprise of a mixed CO adsorption structure at the

atop, bridge and fcc sites. From our results, only when the overall CO coverage at the hollow or bridge site is above 0.325 ML, the pzc can be larger than 1.0 V. In particular, the calculated pzc for the CO coverages at 0.625 ML with mixed adsorption structures (e.g. 0.25T_0.125B_0.25 ML H) can be in between 1.0 and 1.2 V (see Fig. 4), which is in the best agreement with the value (~1.1 V) extrapolated from experiment with the CO coverage about 0.63–0.68 ML. The C_d of CO/Pt(1 1 1) system can be calculated through the slope of the $\sigma \sim U$ curve, similar to that in Fig. 3b. We found that the calculated C_d for the three calculated 0.625 ML CO adsorption structures are almost identical, being about ~14 μF/cm^2. The value is consistent with that measured by Cuesta and coworkers, who obtained the C_d of 15 μF/cm^2 for Pt(1 1 1) [12]. Obviously, unlike that of pzc, C_d value is not very sensitive to the CO adsorption site and coverage. By comparing CO/Pt(1 1 1) with bare Pt(1 1 1), it is clear that the CO adsorption will reduce C_d value slightly but increase markedly the pzc value. Fundamentally, this is be caused by the sensitivity of pzc to the surface dipole and thus the presence of adsorbates, while the C_d value, being the derivative of surface charge versus potential, is less sensitive to the presence of adsorbates.

4.3.1. CO electrooxidation

With no more approximations, the DFT/CM-MPB method can be applied straightforwardly to electrocatalytic reactions at electrode/solution interface. Here we illustrate the method in CO electrocatalytic reactions on Pt(1 1 1), a model reaction in electrochemistry. It is known that CO can be removed from Pt(1 1 1) by elevating the potential: the reaction occurs rapidly (exhibits the major oxidation current peak) only above a certain potential, i.e. ~0.7 V on Pt(1 1 1). It has been a hot debate whether it is O or OH oxidative species on the surface that participates the CO oxidation. Both O and OH can be generated from H_2O oxidation at the high potential on Pt(1 1 1). Theoretically, this requires a direct comparison of the barrier of CO + O → CO_2 and CO + OH → COOH reactions under the electrochemical conditions.

We have utilized the DFT/CM-MPB model to calculate the reaction pathway for the two reactions. The calculated TSs for the two reactions are shown in Fig. 5. For CO + O reaction, the reaction pathway in solution is similar to what is known in the vapor phase, where initially CO and O are at the top and hollow sites and at the TS O moves to a bridge site to react with the off-top site CO. The calculated reaction barrier is 0.66 eV under DFT/CM-MPB model, which is slightly lower than that in vacuum (~0.79 eV) [61], apparently because of a larger solvation contribution of the bridging O (out of the surface) at the TS compared to the hollow site O at the IS. For CO + OH reaction, the reaction is much more facile compared to CO + O reaction, with the calculated barrier being only 0.36 eV [62]. This is largely due to the fact that there is little distinction between the IS and the TS for the CO + OH reaction as CO and OH always stay at the top site with OH solvated by nearby explicit H_2Os. It might be mentioned that the presence of explicit H_2O molecules nearby OH helps to stabilize OH at the IS and the calculated reaction barrier with explicit H_2O is higher by ~0.1 eV. On the other hand, the stabilization to the adsorbed O atom by the presence of explicit H_2O is small [30,40] and thus neglected in CO + O reaction.

We also found that the potential dependence of the reaction barrier of the two reactions are rather small, as shown in Fig. 5, by calculating the reaction barrier under different charge conditions [30,40]. The reaction barriers are rather constant at the potentials concerned, i.e. 0.4–0.9 V. The electrochemical potential does not change significantly the reaction barrier of these surface coupling reactions, which is consistent with our recent results for other surface coupling reactions, such as O coupling (O + O and O + OH) on Pt and RuO_2 [30,40]. Our results indicate that CO electrocatalytic on Pt(1 1 1) should follow the CO + OH reaction channel, not the CO + O channel. The difference in rate at 300 K is estimated to be six orders of magnitude between two channels. Experimentally, Feliu et al. have suggested that OH is the reactive species for CO electrocatalytic oxidation on Pt(1 1 1) using voltammograms technique.

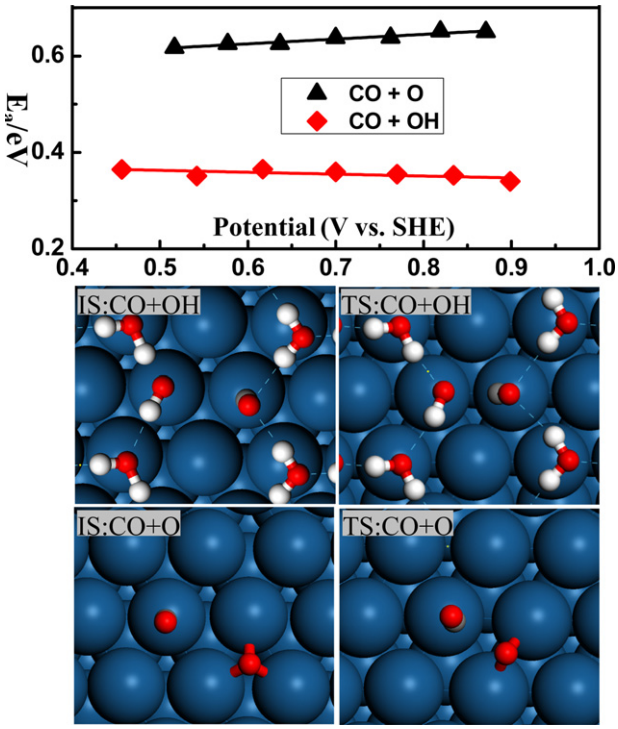

Fig. 5. The variation of the reaction barrier (E_a) at different potentials for CO electrooxidation on Pt(1 1 1) via the CO + O and the CO + OH reaction channels. The optimized structures for the ISs and the TSs are illustrated.

5. Conclusions

This work represents the theoretical progress to describe the electrode/electrolyte interface within the periodic DFT framework by using modified-Poisson–Boltzmann electrostatics to model the electrochemical conditions (e.g. electrochemical potential, solvation, electrolyte distribution etc.). In this theoretical approach, the slab of electrode can be explicitly charged and the ionic distribution of electrolyte is represented by point-charges in continuum dielectric medium, which can be solved self-consistently in the framework of first principles electronic structure calculations.

To validate the method, we have calculated the pzc and C_d of a series of metal electrodes and CO-covered Pt electrode, and the calculated values are found to be in good agreement with experimental measurement. We also extend this approach to electrocatalytic reactions at the metal/solution interface, i.e. CO electrooxidation on Pt(1 1 1). Two different mechanisms are investigated, namely CO reacting with surface O or OH, and CO + OH mechanism is found to be the major coupling channel. We show that the reaction barriers of these surface association reactions have a weak dependence on potential. We demonstrate that the current DFT/CM-MPB method is a methodologically simple and practically feasible tool for studying complex electrochemical systems in general, and can provide important insight into the nature of electrochemical double layer and the catalytic reaction.

Acknowledgements

This work is supported by National Nature Science Foundation of China (20825311, 21173051, 21103110), 973 program (2011CB808500), Science and Technology Commission of Shanghai

Municipality (08DZ2270500), Program for Professor of Special Appointment (Eastern Scholar) and Program for Young Teacher Training (yyy11011) at Shanghai Institute of Higher Learning, Shanghai Institute of Technology Scientific Research Foundation for Introduced Talent (YJ2011-45).

References

[1] A.J. Bard, L.R. Faulkner, Electrochemical Methods – Fundamentals and Applications, 2nd ed., John Wiley & Sons, New York, 2001.
[2] P. Ramirez, A. Granero, R. Andreu, A. Cuesta, W.H. Mulder, J.J. Calvente, Electrochemistry Communications 10 (2008) 1548.
[3] K.A. Soliman, L.A. Kibler, Electrochimica Acta 52 (2007) 5654.
[4] M. Ozawa, M. Hattori, Journal of Alloys and Compounds 408 (2006) 560.
[5] A.M. El-Aziz, R. Hoyer, L.A. Kibler, D.M. Kolb, Electrochimica Acta 51 (2006) 2518.
[6] M. Zic, Journal of Electroanalytical Chemistry 584 (2005) 215.
[7] G. Gouy, Journal de Physique et Le Radium 9 (1910) 457.
[8] D.L. Chapman, Philosophical Magazine 25 (1913) 475.
[9] O. Stern, Zeitschrift für Elektrochemie 30 (1924) 508.
[10] T. Iwasita, X.H. Xia, Journal of Electroanalytical Chemistry 411 (1996) 95.
[11] N. Garcia-Araez, V. Climent, E. Herrero, J.M. Feliu, J. Lipkowski, Electrochimica Acta 51 (2006) 3787.
[12] A. Cuesta, Surface Science 572 (2004) 11.
[13] K.L. Yang, S. Yiacoumi, C. Tsouris, Journal of Chemical Physics 117 (2002) 337.
[14] M. Vossen, F. Forstmann, Journal of Chemical Physics 101 (1994) 2379.
[15] A. Kramer, M. Vossen, F. Forstmann, Journal of Chemical Physics 106 (1997) 2792.
[16] I. Borukhov, D. Andelman, H. Orland, Physical Review Letters 79 (1997) 435.
[17] A. Abrashkin, D. Andelman, H. Orland, Physical Review Letters 99 (2007) 077801.
[18] M.S. Kilic, M.Z. Bazant, A. Ajdari, Physical Review E 75 (2007) 021503.
[19] E. Spohr, K. Heinzinger, Electrochimica Acta 33 (1988) 1211.
[20] J.W. Halley, A. Mazzolo, Y. Zhou, D. Price, Journal of Electroanalytical Chemistry 450 (1998) 273.
[21] O. Sugino, I. Hamada, M. Otani, Y. Morikawa, T. Ikeshoji, Y. Okamoto, Surface Science 601 (2007) 5237.
[22] S. Schnur, A. Gross, New Journal of Physics 11 (2009) 25003.
[23] A.Y. Lozovoi, A. Alavi, J. Kohanoff, R.M. Lynden-Bell, Journal of Chemical Physics 115 (2001) 1661.
[24] J.S. Filhol, M. Neurock, Angewandte Chemie International Edition 45 (2006) 402.
[25] E. Skulason, V. Tripkovie, M.E. Bjorketun, S. Gudmundsdottir, G. Karlberg, J. Rossmeisl, T. Bligaard, H. Jonsson, J.K. Norskov, Journal of Physical Chemistry C 114 (2010) 18182.
[26] C.D. Taylor, M. Neurock, Current Opinion in Solid State and Materials Science 9 (2005) 49.
[27] S. Trasatti, E. Lust, Modern aspects of electrochemistry, in: A.E.B. White, J.O'M.B.E. Conway (Eds.), The Potential of Zero Charge, vol. 33, Kluwer Academic/Plenum Publishers, New York, Boston, Dordrecht, London, Moscow, 2002, pp. 1–303.
[28] C.D. Taylor, R.G. Kelly, M. Neurock, Journal of Electroanalytical Chemistry 607 (2007) 167.
[29] R. Jinnouchi, A.B. Anderson, Physical Review B 77 (2008) 245417.
[30] Y.H. Fang, Z.P. Liu, Journal of the American Chemical Society 132 (2010) 18214.
[31] R. Jinnouchi, A.B. Anderson, Journal of Physical Chemistry C 112 (2008) 8747.
[32] Y.F. Li, Z.P. Liu, L.L. Liu, W.G. Gao, Journal of the American Chemical Society 132 (2010) 13008.
[33] J.M. Soler, E. Artacho, J.D. Gale, A. Garcia, J. Junquera, P. Ordejon, D. Sanchez-Portal, Journal of Physics: Condensed Matter 14 (2002) 2745.
[34] J. Junquera, O. Paz, D. Sanchez-Portal, E. Artacho, Physical Review B 64 (2001) 235111.
[35] N. Troullier, J.L. Martins, Physical Review B 43 (1991) 1993.
[36] J.P. Perdew, K. Burke, M. Ernzerhof, Physical Review Letters 77 (1996) 3865.
[37] S. Garcia-Gil, A. Garcia, N. Lorente, P. Ordejon, Physical Review B 79 (2009) 5441.
[38] H.F. Wang, Z.P. Liu, Journal of the American Chemical Society 130 (2008) 10996.
[39] C. Shang, Z.P. Liu, Journal of Chemical Theory and Computation 6 (2010) 1136.
[40] Y.H. Fang, Z.P. Liu, Journal of Physical Chemistry C 113 (2009) 9765.
[41] H.F. Wang, Z.P. Liu, Journal of Physical Chemistry C 113 (2009) 17502.
[42] J.L. Fattebert, F. Gygi, Journal of Computational Chemistry 23 (2002) 662.
[43] C.J. Cramer, D.G. Truhlar, Chemical Reviews 99 (1999) 2161.
[44] Y.H. Fang, Z.P. Liu, Journal of Physical Chemistry C 114 (2010) 4057.
[45] B. Fornberg, D.M. Sloan, Acta Numerica 3 (1994) 203.
[46] S. Trasatti, Electrochimica Acta 36 (1991) 1659.
[47] V. Climent, G.A. Attard, J.M. Feliu, Journal of Electroanalytical Chemistry 532 (2002) 67.
[48] T. Pajkossy, D.M. Kolb, Electrochemistry Communications 5 (2003) 283.
[49] J.L.F. Da Silva, C. Stampfl, M. Scheffler, Surface Science 600 (2006) 703.
[50] D.R. Lide, CRC Handbook of Chemistry and Physics, 84th ed., CRC Press, 2003–2004.
[51] P. Brault, H. Range, J. Toennies, C. Woll, Zeitschrift fur Physikalische Chemie 198 (1997) 1.
[52] D.M. Kolb, Angewandte Chemie International Edition 40 (2001) 1162.
[53] J.O.M. Bockris, S.U.M. Khan, Quantum Electrochemistry, Plenum Press, New York, London, 1979.
[54] D.C. Grahame, Chemical Reviews 41 (1947) 441.
[55] N.P. Lebedeva, M.T.M. Koper, J.M. Feliu, R.A. van Santen, Journal of Electroanalytical Chemistry 524 (2002) 242.
[56] D.S. Strmcnik, D.V. Tripkovic, D. van der Vliet, K.C. Chang, V. Komanicky, H. You, G. Karapetrov, J.P. Greeley, V.R. Stamenkovic, N.M. Markovic, Journal of the American Chemical Society 130 (2008) 15332.
[57] A. Lopez-Cudero, A. Cuesta, C. Gutierrez, Journal of Electroanalytical Chemistry 586 (2006) 204.
[58] I. Villegas, M.J. Weaver, Journal of Chemical Physics 101 (1994) 1648.
[59] M.B. Song, K. Yoshimi, M. Ito, Chemical Physics Letters 263 (1996) 585.
[60] M.J. Weaver, S.Z. Zou, C. Tang, Journal of Chemical Physics 111 (1999) 368.
[61] X.Q. Gong, Z.P. Liu, R. Raval, P. Hu, Journal of the American Chemical Society 126 (2004) 8.
[62] X.Q. Gong, P. Hu, R. Raval, Journal of Chemical Physics 119 (2003) 6324.